Supporting Information

$MoP_4/Ni_3S_2/MoO_3$ heterogeneous structure nanorod arrays for efficient solar-enhanced overall water splitting

Yikun Cheng[a], Pengjie Fu[b], Xiaodong Yang[b,*], Yangrui Zhang[a], Shan Jin[a], Huan Liu[a], Yunfei Shen[a], Xuhong Guo[*, a,c], Long Chen[*, a]

[a] School of Chemistry and Chemical Engineering/State Key Laboratory Incubation Base for Green Processing of Chemical Engineering, Shihezi University, Shihezi 832003, China.

[b] College of Science, Shihezi University, Shihezi 832003, China.

[c] State Key Laboratory of Chemical Engineering, East China University of Science and Technology, Shanghai 200237, China.

First author

E-mail address: 1754394006@qq.com

* Corresponding authors

E-mail address: chenlong2012@sinano.ac.cn (L. Chen)

E-mail address: yangxiaodong1209@hotmail.com (X. Yang)

E-mail address: guoxuhong@ecust.edu.cn (X. H. Guo)

Experimental section

1.1 Material

All the chemicals were directly used after purchase without further purification: ammonium molybdate tetrahydrate ($(NH_4)_6Mo_7O_{24}\cdot 4H_2O$, 99.9%), nickel(II) chloride hexahydrate ($NiCl_2\cdot 6H_2O$, 99.9%), sodium hypophosphite ($NaH_2PO_2\cdot H_2O$, 98%),

sulfur powder (99.9%), ethanol absolute (99.5%), deionized water (self-prepared by deionized water machine), potassium hydroxide (KOH, 98%), commercial Pt/carbon (20 wt %) and ruthenium(IV) oxide (99.9%). Nickel foam (NF, thickness 1.6 mm, 95%) was cut into the size of 1 × 3 cm, then washed with 1 M hydrochloric acid (HCl) solution, ethanol absolute, and deionized water under ultrasonication for 15 min to remove the surface oxide layer and organic residue, respectively. After cleaning with deionized water, the NF was dried in a vacuum oven for 12 h at 60^{o}C.

1.2 Material synthesis

Preparation of Pt/C electrode on Ni foam:

The commercial Pt/C (20 mg) was mixed with 500 μL ethanol, 480 μL deionized water and 20 μL Nafion solution, and the mixture was ultrasonicated for 30 min to obtain a homogeneous dispersion. Then the dispersed solution was coated onto nickel foam, followed with the dry in air at room temperature. The loading amount of Pt/C catalyst on the Ni foam is about 4.8 mg cm^{-2}.

Preparation of RuO_2 electrode on Ni foam:

20 mg RuO_2, 20 μL Nafion solution, 500 μL ethanol and 480 μL deionized water were mixed with ultrasonicated for 30 min to obtain a homogeneous dispersion. Then the dispersion solution was coated onto nickel foam, followed by the dry in air at room temperature. The loading of RuO_2 on Ni foam is about 4.5 mg cm^{-2}.

1.3 Material Characterization

The materials (NiMo-PS@NF, NiMo-P@NF, NiMo-S@NF, and NiMo@NF) electrodes synthesized are reflected by X-ray powder diffractometry (XRD), wherein

Cu Kα radiation (λ = 0.15406 nm) 2 theta ranged from 5 to 90°. The surface morphology was characterized by scanning electron microscopy (SEM) (ZEISS MERLIN Compact, Germany) and transmission electron microscopy (TEM) (FEI, Tecnai G2 F20 S-Twin, America). Raman spectroscopy was recorded using a STEX-100 Compact Confocal Raman spectrometer at 532 nm an argon ion laser as the excitation source. X-ray photoelectron spectroscopy (XPS) (Thermo, ESCALAB 250XI, America) analyses were conducted on an equipped with a focused monochromatic Al Kα X-ray S-3 source. The peak energies were calibrated by placing the major C 1s peak at 284.8 eV.

1.4 Electrochemical Measurements

1.4.1 Evaluation of the electrocatalytic activity toward HER and OER

The electrochemical test of oxygen evolution reaction (OER) and hydrogen evolution reaction (HER) are performed at CHI760e electrochemical workstation (CHI 760E, CH Instruments Inc., Shanghai, China). Using Graphite rods, Hg/HgO, and materials (NiMo-PS@NF, NiMo-P@NF, NiMo-S@NF, and NiMo@NF) electrodes as the counter electrode, reference electrode, and the working electrode, respectively. The reaction condition is at 1 M KOH electrolyte 25°C. The plots of electrochemical impedance spectroscopy (EIS) were collected at an overpotential of 211.8 mV in the frequency of 0.1 Hz ~ 100 kHz. The LSV curves test for both HER and OER at the scan rate of 5 mV s^{-1}. The LSV curves for the OER reaction were recorded on a voltage of 0.9 to 0.1 V and the HER was recorded at -0.9 to -1.6 V. All measured potentials are referred to as reversible hydrogen electrodes (RHE) in 1 M KOH by RHE calibration, as shown in the following equation:

$$E_{(RHE)} = E_{(Hg/HgO)} + 0.098\ V + 0.0592 \times pH \quad (1)$$

The overpotential (η) for HER and OER are calculated according to the following formulations[1]:

$$\eta_{(OER)} = E_{(RHE)} - 1.23 \quad (2)$$

$$\eta_{(HER)} = E_{(RHE)} \quad (3)$$

1.4.2 Solar-enhanced electrochemical test

For LSV and EIS tests, the working electrode is irradiated under a 500 W Xenon lamp (CHF-XM500) with an AM 1.5G filter. The simulated light intensity is 250 mW cm^{-2} controlled with an optical power meter (PL-MW 2000). Other operations are the same as 1.3.1.

1.4.3 Calculations of ECSA

The ECSA values of the NiMo-PS@NF, NiMo-P@NF, NiMo-S@NF, and NiMo@NF catalysts were estimated according to the method reported elsewhere[2,3]. The double layer capacitance (Cdl) of catalysts was firstly determined on the basis of the current density versus the scan rate plots in the region of -0.25 to -0.35 V, in which no significant Faradaic processes were observed. The electrochemical surface area (ECSA) of the catalyst was calculated from the Coulombic charge Q for hydrogen desorption based on the equation:

$$ECSA = C_{dl}/C_s \quad (4)$$

Where C_{dl} is the calculated double layer capacitance of the as-prepared samples in 1.0 M KOH (in mF cm^{-2}), C_s is the specific capacitance for a flat surface (40 μF cm^{-2} was used here).

1.4.4 Calculation of turnover frequency (TOF)

The TOF calculation of HER is according to the following equation:

$$TOF = j/2Fn \quad (5)$$

where j is the measured current density corresponding to the specific overpotential in the HER process. n is the number of active sites (mol cm^{-2}) and F is the Faraday constant (96485 C mol^{-1}). Factor 1/2 is presented because two electrons are required to form one hydrogen molecule. The number of active sites is obtained from the widely used CV method (Figure S7a-d). Specifically, the CV curves are performed with the potential window range from 0 V to 0.6 V vs. RHE at a scan rate of 50 mV s^{-1} in 1.0 M PBS (pH=7.2). Then, the surface charge density (Q_s) can be obtained by integrating the CV curve's charge over the whole potential range, the half value of the charge is the Q_s. After this, the n value can be calculated according to $n = Q_s/F$. Hence, the n of NiMo-PS@NF, NiMo-S@NF, NiMo-P@NF, and NiMo@NF are $3.76*10^{-6}$, $9.82*10^{-6}$, $6.42*10^{-6}$ and $5.79*10^{-6}$ mol cm^{-2}, respectively.

The computational formula for TOF of OER was (6), j - current density (A cm^{-2}); A - surface area (1 cm^{-2}) of electrodes; F - Faraday constant (96485 C mol^{-1}), and m - amounts of active sites in the catalysts (mol cm^{-2})[4,5].

$$TOF = \frac{j * A}{4 * F * m} \quad (6)$$

The mounts of active sites in the catalysts (m) are obtained by the following formulation, where n - the number of electrons transport (n = 1), R - ideal gas constant, and T - absolute temperature, m is obtained by the following formulation.

$$\text{slope} = \frac{n^2 * F^2 * A * m}{4 * R * T} \quad (7)$$

1.4.5 Evaluation of Faradic efficiency

The Faradic efficiency of NiMo-PS@NF electrocatalysts is estimated by collecting the amount of O_2 and H_2 produced by continuous electrolysis at 100 mA cm^{-2} for about 30 min by volumetric method (V_{actual}). Then, the theoretical generated O_2/H_2 volumes values ($V_{theoretical}$) are calculated by Faraday's law of electrolysis ($Q = N_{O_2/H_2} \times F \times Z$) and Ideal Gas Law ($PV_{O_2/H_2} = N_{O_2/H_2} \times R \times T$). Finally, the Faradaic efficiency is obtained by comparing the actual volume of oxygen evolution with the theoretical one: $FE = V_{actual} / V_{theoretical}$[6]

1.4.6 STH Conversion Efficiency Calculation

For the overall water splitting system that produces hydrogen and oxygen molecules using only commercial silicon solar cell as the input, the solar-to-hydrogen conversion efficiency (STH) is defined as[40]:

$$STH = \frac{Chemical\ energy\ output}{Solar\ energy\ input} = \frac{j_{op}\ x\ A\ x\ E_f\ x\ FE_{H2}}{P_s\ x\ A} = \frac{1.23 x j_{op}}{P_s} x 100\% \quad (8)$$

Here, j_{op} represents the operating current density of the combined system, A is the effective illuminated area, E_f is the standard thermodynamic potential difference between hydrogen evolution and oxygen evolution half-reactions (1.23 V) that is corresponded to the change of Gibbs free energy of overall water splitting, FE_{H2} is the faradic efficiency for hydrogen evolution and P_s is the power of solar illumination (AM 1.5G 100 mW cm^{-2}).

1.5 DFT Computational Details

In this work, The density functional theory (DFT) method was employed to obtain

the geometric optimizations using the Vienna ab initio simulation package (VASP) [41,42]. To improve the calculation efficiency, projector augmented wave (PAW) pseudopotentials were employed to describe the interaction between valence and core electrons [43,44]. The generalized gradient approximation (GGA) of the Perdew-Burke-Ernzerhof (PBE) functional is used as the exchange-correlation functional [45-47]. To prevent interactions between adjacent periodic images, a vacuum region exceeding 20 Å along the z-axis was included. The MoP_4/MoO_3, $MoP_4/Ni_3S_2/MoO_3$, $MoP_4/NiMoO_4$, Ni_3S_2/MoO_3, $Ni_3S_2/NiMoO_4$ heterojunction models were constructed for simulation purposes (all crystal planes are (001) planes), and the Brillouin zone was sampled using a 4 × 4 × 1 grid centered at the gamma (Γ) point in reciprocal space for structure optimization [48]. An energy cutoff of 450 eV was applied for the plane-wave expansion of the electronic eigenfunctions. The geometry optimization was done with a convergence tolerance of 10^{-5} eV for the total energy and all the atoms were allowed to relax until the force was less than 0.05 eV/Å. The van der Waals interaction was determined using Grimme's semiempirical dispersion-corrected DFT-D3 scheme [49,50].

$$E_{ads} = E_{total} - E_{substrate} - E_{adsorbate} \quad (8)$$

where E_{ads} is the adsorption energy of the system, Etotal, Esubstrate, and Eadsorbate are the total system energy, catalyst, and adsorption energy, respectively.

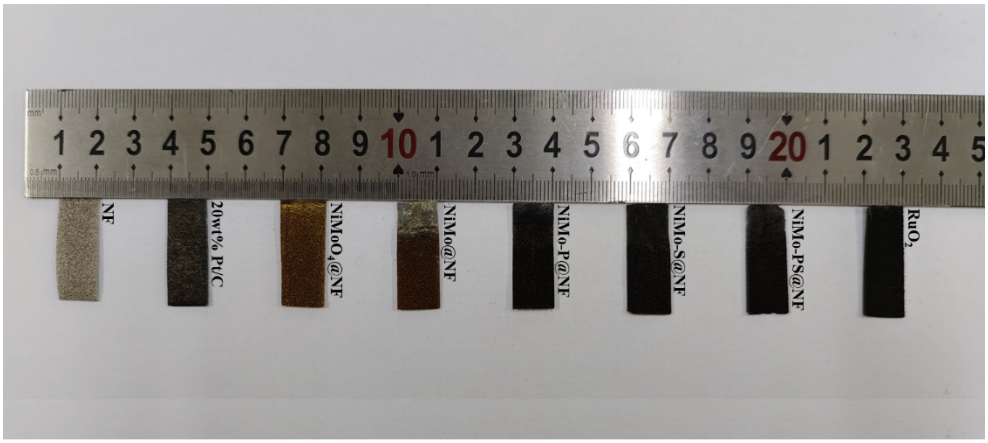

Figure S1. Digital image of NF, 20wt% Pt/C, $NiMoO_4$/NF, NiMo@NF, NiMo-P@NF, NiMo-S@NF, NiMo-PS@NF, and RuO_2 catalysts.

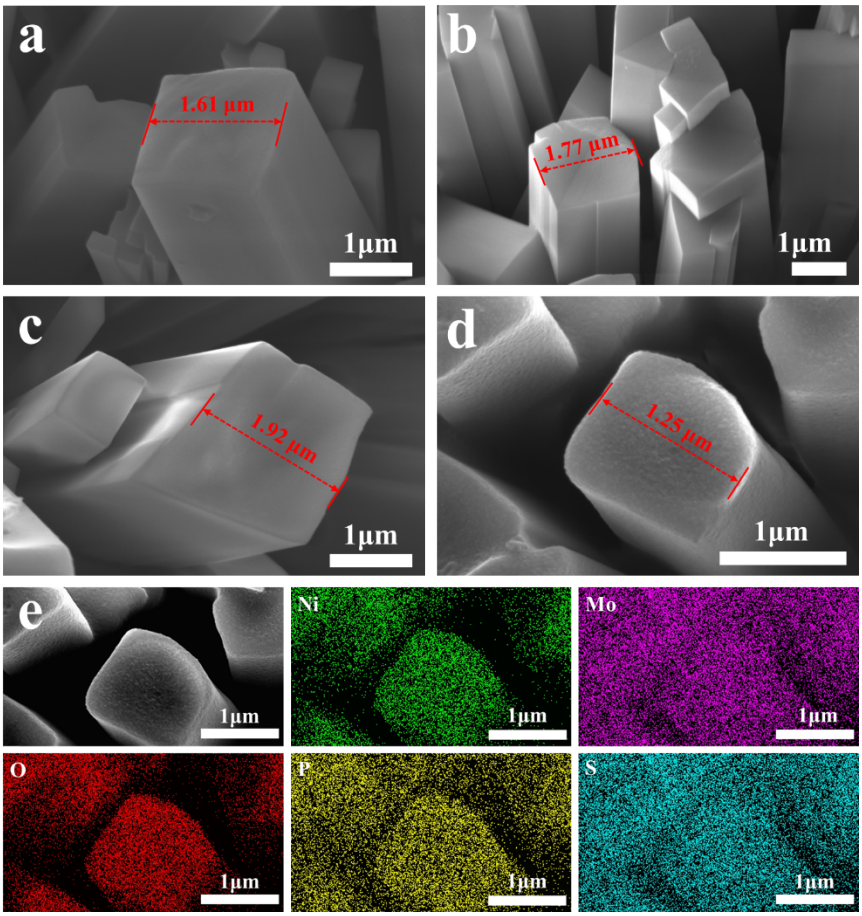

Figure S2. (a-d) SEM images of NiMo@NF, NiMo-P@NF, NiMo-S@NF, and NiMo-PS@NF. (e) EDS elemental mapping images of NiMo-PS@NF.

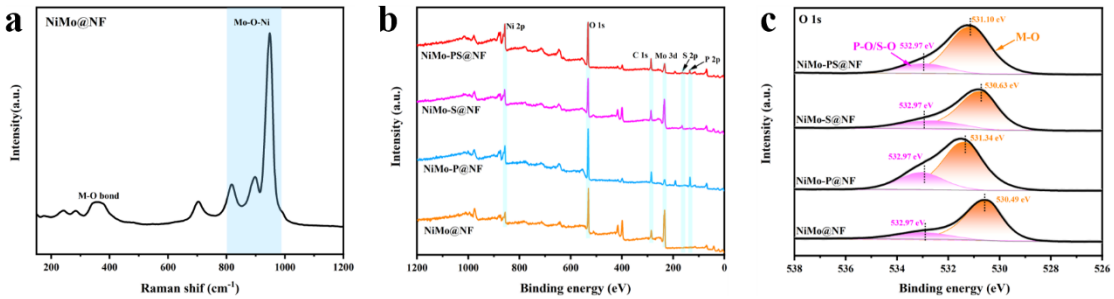

Figure S3. (a) Raman spectra of NiMo@NF. (b) XPS survey spectrum of NiMo@NF, NiMo-P@NF, NiMo-S@NF, and NiMo-PS@NF. (c) O 1s high-resolution XPS spectra of NiMo@NF, NiMo-P@NF, NiMo-S@NF, and NiMo-PS@NF.

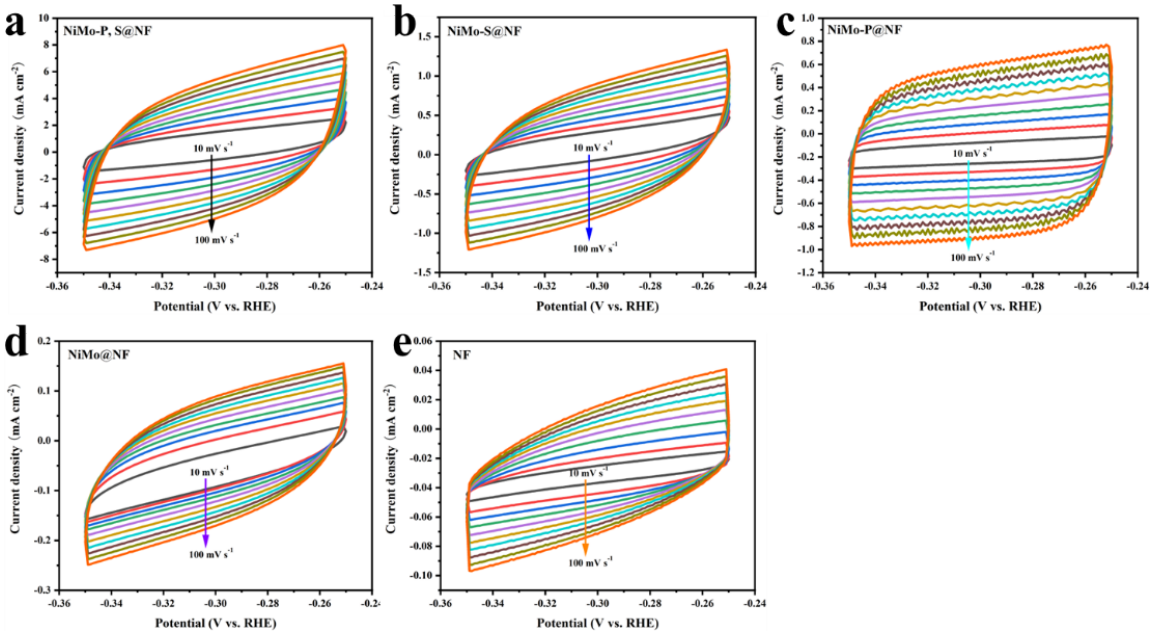

Figure S4. CV curves of (a) NiMo-PS@NF, (b) NiMo-S@NF, (c) NiMo-P@NF, (d) NiMo@NF, and (e) NF at different scan rates in 1 M KOH.

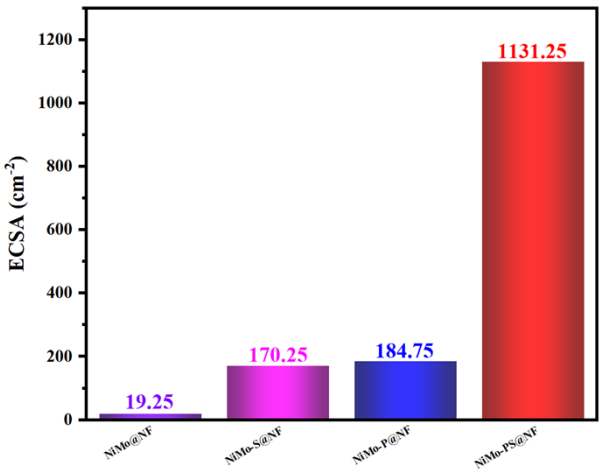

159 Figure S5. ECSA values of NiMo-PS@NF, NiMo-S@NF, NiMo-P@NF, and

160 NiMo@NF in HER test.

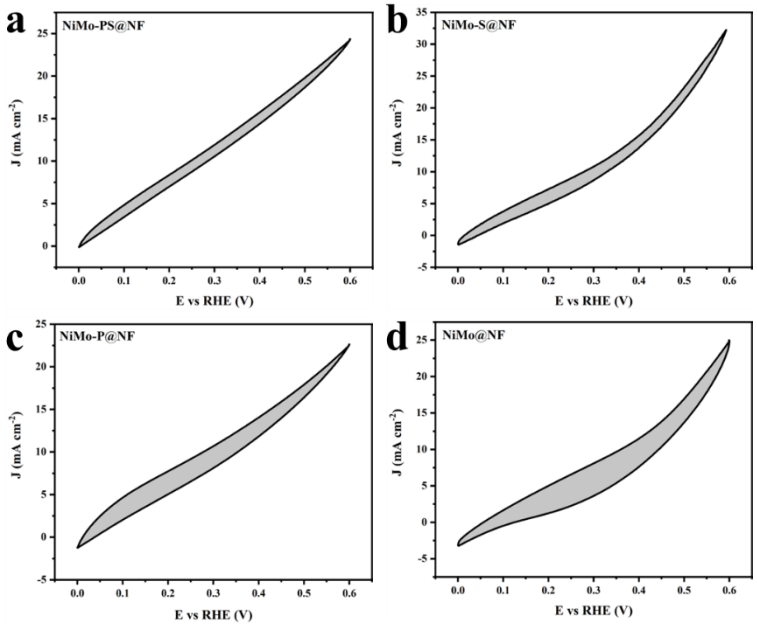

161 Figure S6. CV curves of (a) NiMo-PS@NF, (b) NiMo-S@NF, (c) NiMo-P@NF, and

162 (d) NiMo@NF in 1.0 M PBS at a scan rate of 50 mV s^{-1}.

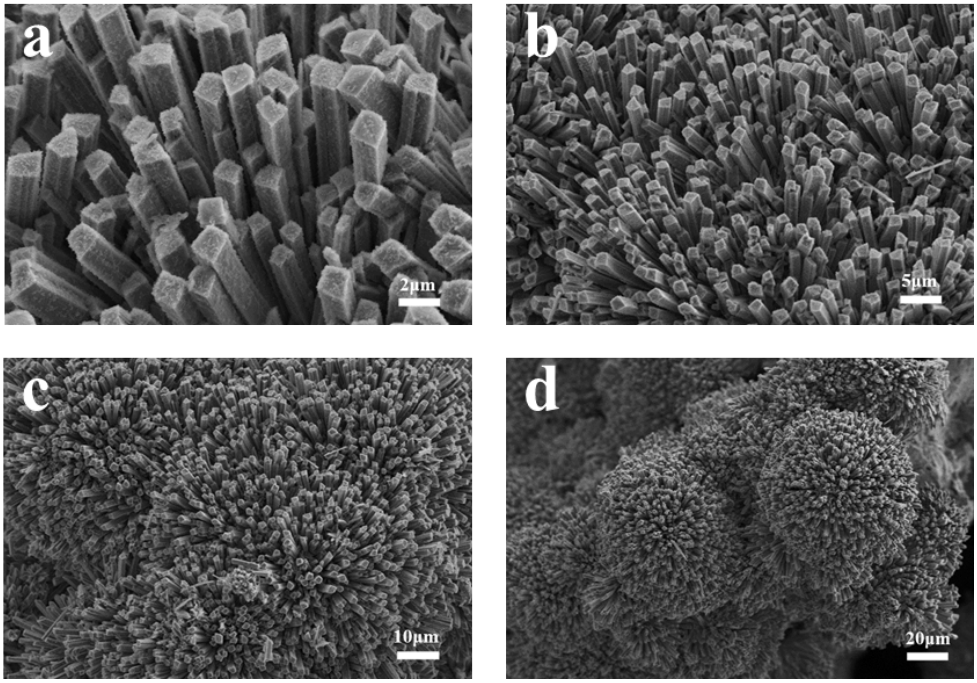

163 Figure S7. (a-d) SEM images of NiMo-PS@NF after HER long-term stability test.

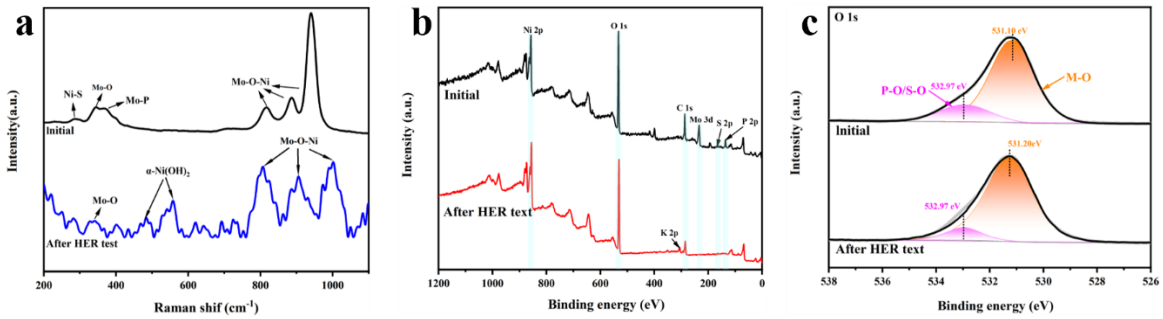

164 Figure S8. (a) Raman spectra of NiMo-PS@NF after HER long-term stability test. (b)

165 XPS survey spectrum and (c) O 1s high-resolution XPS spectra of NiMo-PS@NF

166 before and after HER long-term stability test.

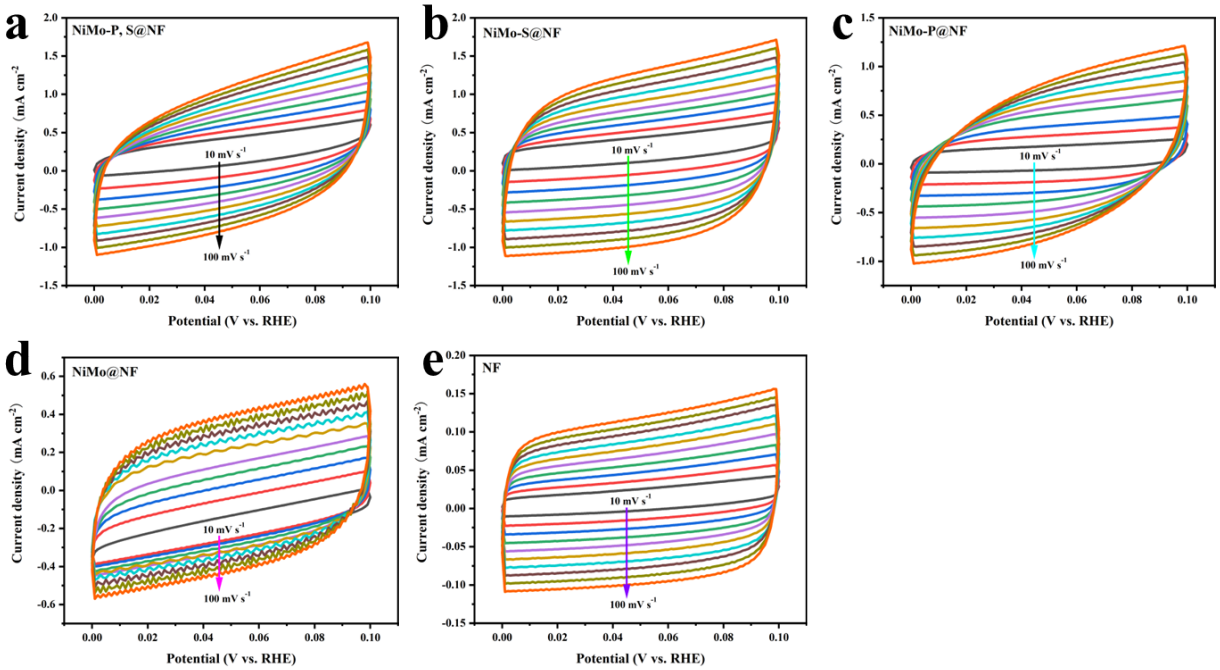

167 Figure S9. CV curves at different scan rates of (a) NiMo-PS@NF, (b) NiMo-S@NF,

168 (c) NiMo-P@NF, (d) NiMo@NF, and (e) NF.

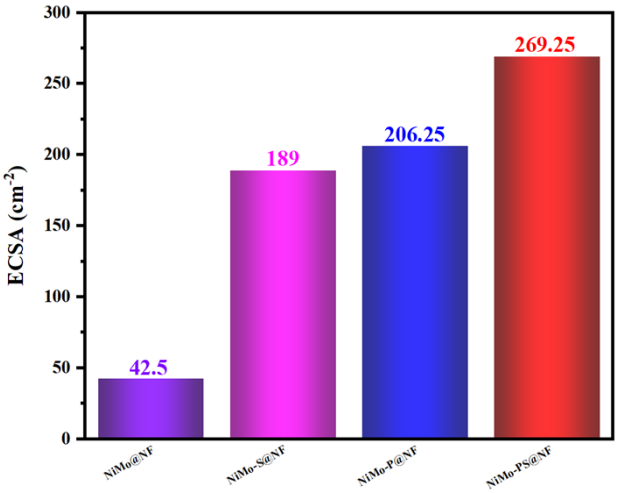

169 Figure S10. ECSA values of NiMo-PS@NF, NiMo-S@NF, NiMo-P@NF, and

NiMo@NF in OER test.

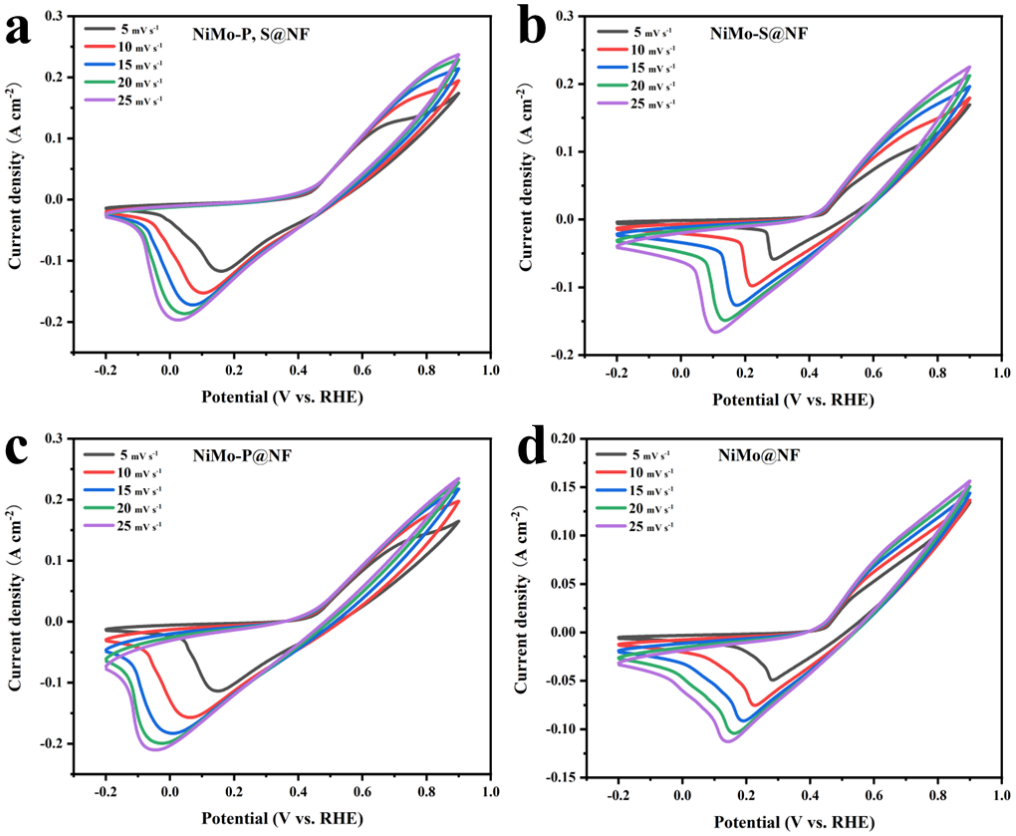

Figure S11. CV of (a) NiMo-PS@NF, (b) NiMo-S@NF, (c) NiMo-P@NF and (d) NiMo@NF at different scan rates of 5, 10, 15, 20, and 25 mV s^{-1} in 1 M KOH.

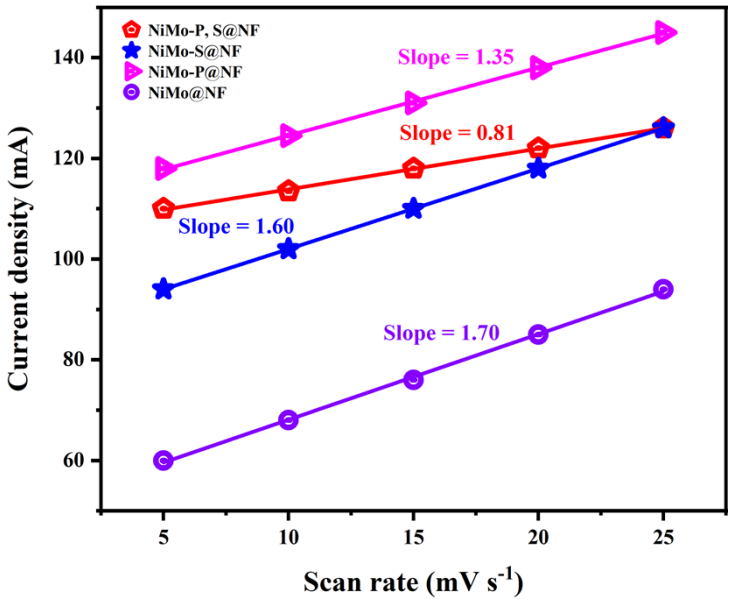

173 Figure S12. Linear relationship of the oxidation peak currents vs. scan rate in the CV

174 of Figure S12a-d.

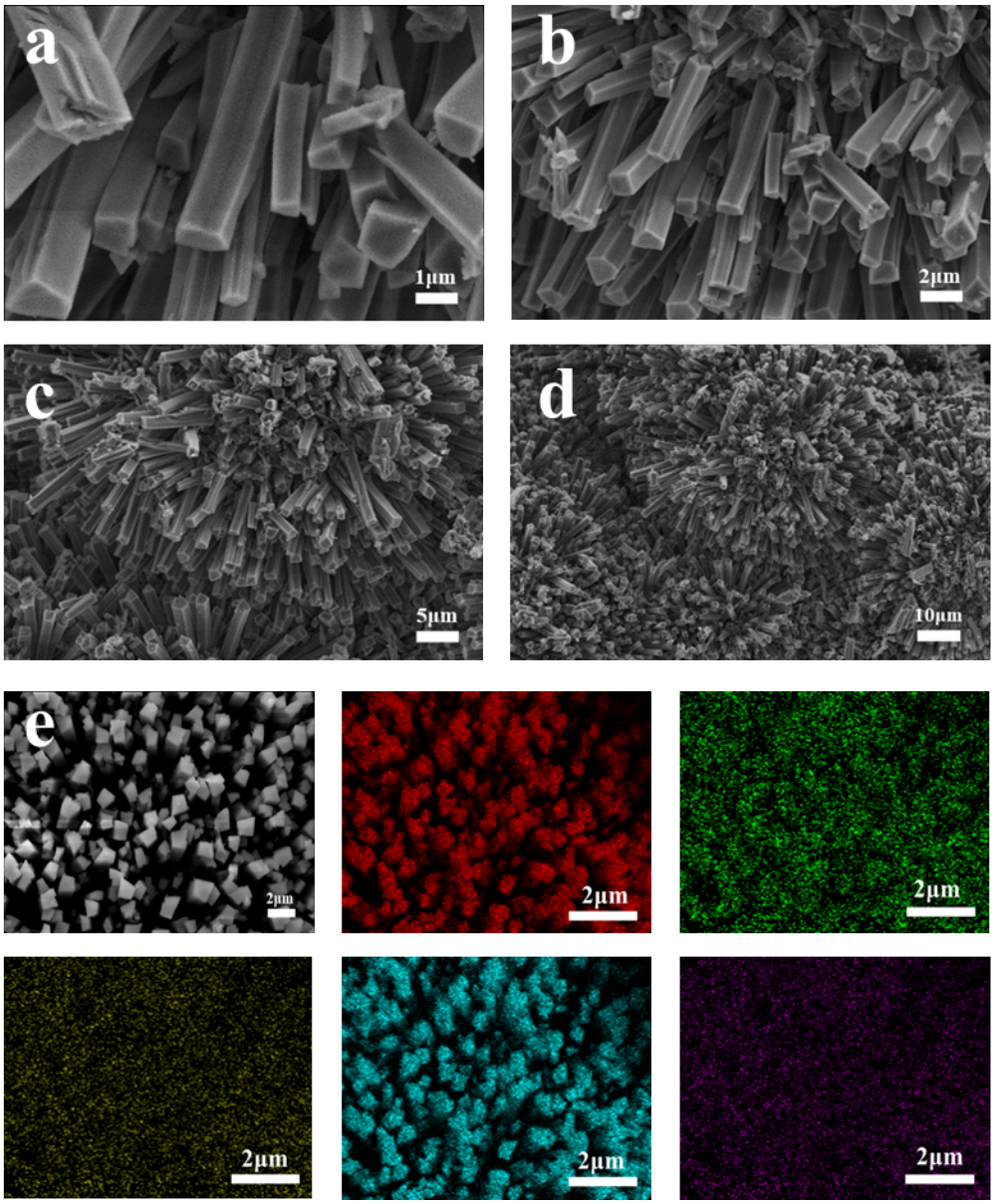

Figure S13. (a-d) SEM images, (e) EDS elemental mapping images of NiMo-PS@NF after OER long-term stability test.

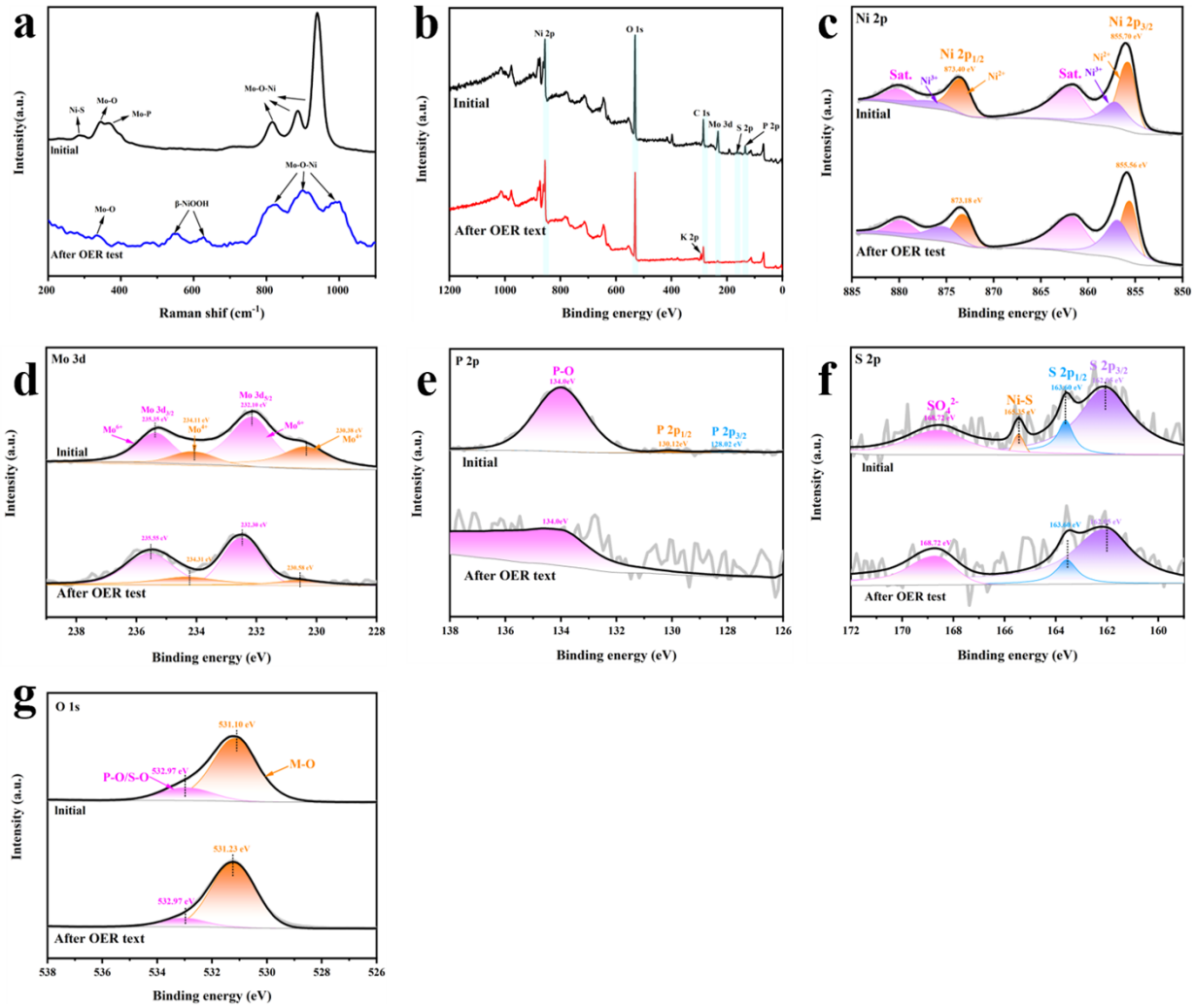

177 Figure S14. (a) Raman spectra, (b) XPS survey spectrum, and high-resolution XPS

178 spectra of (c) Ni 2p, (d) Mo 3d, (e) P 2p, (f) S 2p and (g) O 1s of NiMo-PS@NF before

179 and after OER long-term stability test.

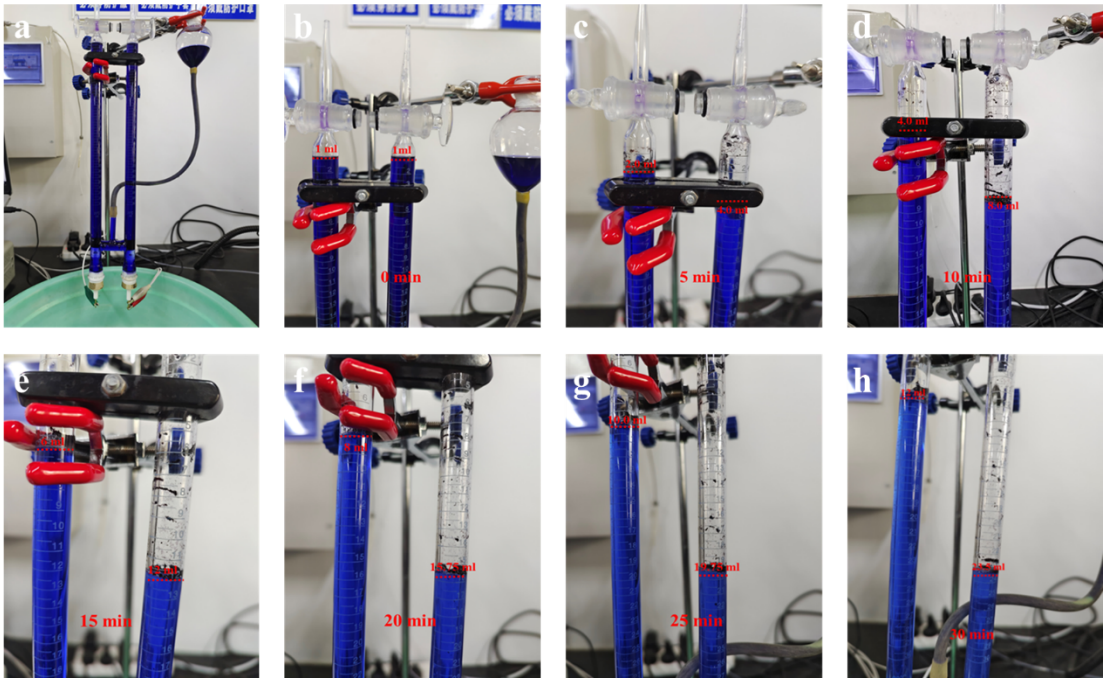

Figure S15. (a-h) A series of digital photograph of the Hoffman apparatus was used for the measurement of the Faradaic efficiency at 100 mA cm^{-2}.

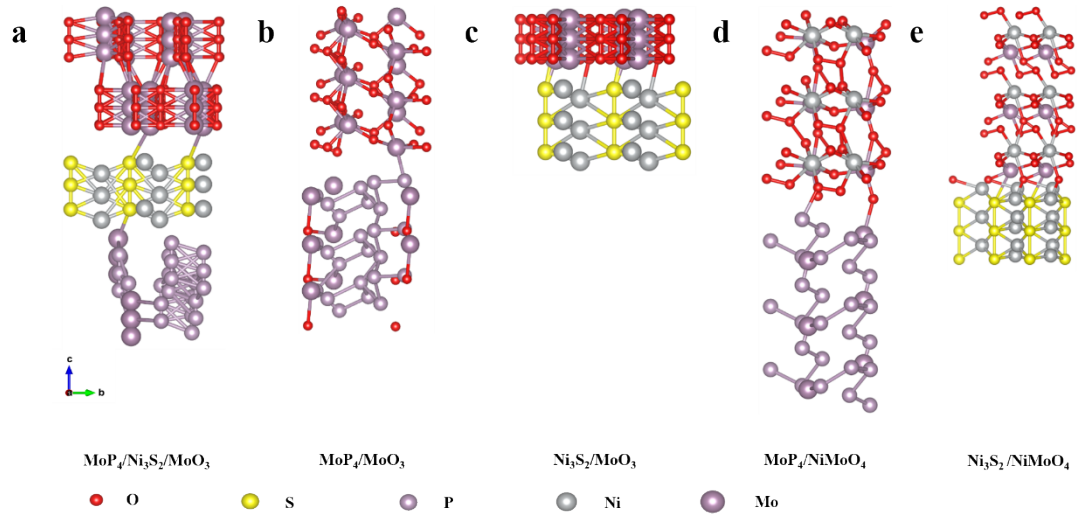

Figure S16. (a-e) $MoP_4/Ni_3S_2/MoO_3$, MoP_4/MoO_3, Ni_3S_2/MoO_3, $MoP_4/NiMoO_4$, and $Ni_3S_2/NiMoO_4$ heterostructures of Schematic models.

Table S1. The impedance value for different samples for HER

Electrocatalysts	R_s (Ω)
NiMo-PS@NF -Light on	1.45
NiMo-PS@NF-Light off	2.31
NiMo-S@NF	4.23
NiMo-P@NF	6.04
NiMo@NF	12.62
NF	50.11

Table S2. The impedance value for different samples for OER

Electrocatalysts	R_s (Ω)
NiMo-PS@NF-Light on	0.96
NiMo-PS@NF-Light off	1.6
NiMo-S@NF	1.74
NiMo-P@NF	1.99
NiMo@NF	9.16
NF	63.88

Table S3. Comparison of electrocatalytic HER activity of recently reported electrocatalysts in 1 M KOH electrolyte.

Catalysts	j (mA cm^{-2})	η (mV)	References
NiMo-PS@NF	10	35	This work
$Mn_3(PO_4)_2$	10	109	Appl. Catal. B, 2021[7]
Ni-Mo_2C@NPC	10	144	Appl. Catal. B, 2022[8]
Mo-NiP_x/NiS_y	10	85	Adv. Funct. Mater., 2021[9]
$CoNi_2S_4$/WS_2/Co_9S_8	10	70	Appl. Catal. B, 2021[10]
$Ru_{0.10}$@2H-MoS_2	10	51	Appl. Catal. B, 2021[11]
CuNi@NiFeCu	10	42	Appl. Catal. B, 2021[12]
Au/Ni_3S_2/NF	10	97	Appl. Catal. B, 2022[13]
$NiSe_2$/Ni_3Se_4/NF-4	10	145	Appl. Catal. B, 2021[14]
NC/Ni-Mo-N/NF	10	72	Appl. Catal. B, 2021[15]
MoS_2/CoSAs-NS-CNTs@CoS_2/CC	10	56	Appl. Catal. B, 2023[16]
Co/CoP@HOMC	10	120	Adv. Energy Mater., 2021[17]
La-MoP@NC	10	129.3	Appl. Catal. B, 2021[18]
SLC	10	51	Appl. Catal. B, 2021[19]
MoP-Ru_2P/NPC	10	47	Appl. Catal. B, 2021[20]
Ni_2P-Ru_2P/NF	10	101	Appl. Catal. B, 2021[21]

Table S4. Comparison of electrocatalytic OER activity of recently reported electrocatalysts in 1 M KOH electrolyte.

Catalysts	j (mA cm-2)	η (mV)	References
NiMo-PS@NF	100	288.8	This work
	10	211.8	
NiFeP/MXene	10	286	Sci. Bull., 2021[22]
$Au/Ni_3S_2/NF$	10	230	Appl. Catal. B, 2022[13]
$Mn_{1.5}Co_{1.5}(PO_4)_2$	10	254	Appl. Catal. B, 2021[7]
$Co(OH)_2$/NiMo CA@CC	10	267	Adv. Funct. Mater., 2021[23]
$Fe_{0.6}Co_{0.4}Se_2$	10	270	Energy Environ. Sci., 2021[24]
NiCoFe-NDA/NF	10	215	Energy Environ. Sci., 2021[25]
CoMoOS-100	10	281	Appl. Catal. B, 202026
CM (1:0.1)	10	300	Sci. Bull., 2020[27]
Co/CoP@HOMC	10	260	Adv. Energy Mater., 2021[17]
Co@N-CS/N-HCP@CC	10	248	Adv. Energy Mater., 2019[28]
$(Ru-Ni)O_x$	10	237.2	Appl. Catal. B, 2021[29]
NCO-Ag-4.1V	10	297	Appl. Catal. B, 2021[30]
so-Fe-$Ni(OH)_2$ TTAs with 45.7 at% Fe	10	226	Appl. Catal. B, 2021[31]
CoP-B1	10	297	Appl. Catal. B, 2021[32]

A-$FeCoSeO_x$-100 HoNPrs	10	294	Appl. Catal. B, 2020[33]

Table S5. Comparison of electrocatalytic overall water splitting activity of recently reported electrocatalysts in 1 M KOH electrolyte.

Catalysts	J ($mA\ cm^{-2}$)	Potential (V)	References
NiMo-PS@NF|| NiMo-PS@NF	10 100	1.391 1.711	This work
Pt/C||RuO_2	10	1.571	
(Ru-Ni)O_x//(Ru-Ni)O_x	10	1.48	Appl. Catal. B, 2021[29]
Co@N-CS/N-HCP@CC// Co@N-CS/N-HCP@CC	10	1.545	Adv. Energy Mater., 2019[28]
Mo-Ni_3S_2/Ni_xP_y/NF//Mo-Ni_3S_2/Ni_xP_y/NF	10	1.46	Adv. Energy Mater., 2020[34]
NiFeP/MXene//Pt/C	10	1.61	Sci. Bull., 2021[22]
$Mn_{1.5}Co_{1.5}$//$Mn_{1.5}Co_{1.5}$	10	1.54	Appl. Catal. B, 2021[7]
SLC//SLC	10	1.49	Appl. Catal. B, 2021[19]
CuNi@Ni-FeCu/CP//	10	1.51	Appl. Catal. B, 2021[12]

CuNi@Ni-FeCu/CP			
Co/CoP@HOMC// Co/CoP@HOMC	10	1.54	Adv. Energy Mater., 2021[17]
Au/Ni_3S_2/NF// Au/Ni_3S_2/NF	10	1.52	Appl. Catal. B, 2022[13]
Mo_2C-CoO@N-CNFs// Mo_2C-CoO@N-CNFs	10	1.56	Chem. Eng. J., 2023[35]
Co@$CoMoO_x$-α-CrOOH/NF// Co@$CoMoO_x$-α-CrOOH/NF	10	1.57	Chem. Eng. J., 2023[36]
Ni($S_{0.5}1Se_{0.49}$)$_2$@NC// Ni($S_{0.5}1Se_{0.49}$)$_2$@NC	10	1.59	Adv. Funct. Mater., 2022[37]
Ni/$NiFe_2O_4$@PPy// Ni/$NiFe_2O_4$@PPy	10	1.64	Chem. Eng. J., 2023[38]
NiFe//MoP-Ru_2P/NPC-NiFe	10	1.49	Appl. Catal. B, 2021[20]
Ni_2P-Ru_2P/NF//Ni_2P-Ru_2P/NF	10	1.45	Appl. Catal. B, 2021[21]
$NiSe_2$/Ni_3Se_4/NF-1//$NiSe_2$/Ni_3Se_4/NF-4	10	1.56	Appl. Catal. B, 2022[39]

References

[1] Y. Luo, X. Yang, L. He, Y. Zheng, J. Pang, L. Wang, R. Jiang, J. Hou, X. Guo and L. Chen, ACS Appl. Mater. Interfaces, 2022, **14**, 46374-46385.

2 W. He, X. Zheng, J. Peng, H. Dong, J. Wang and W. Zhao, Chem. Eng. J., 2020, **396**, 125227.

3 J. Zhu, S. Li, M. Xiao, X. Zhao, G. Li, Z. Bai, M. Li, Y. Hu, R. Feng, W. Liu, R. Gao, D. Su, A. Yu and Z. Chen, Nano Energy, 2020, **77**, 105212.

4 X. Wu, J. Qiu and Z. Wang, Small Struct., 2022, **4**, 42200268.

5 Z. Wang, J. Zhang, Q. Yu, H. Yang, X. Chen, X. Yuan, K. Huang and X. Xiong, Chem. Eng. J., 2021, **410**, 128366.

6 J. Han, J. Zhang, T. Wang, Q. Xiong, W. Wang, L. Cao and B. Dong, ACS Sustain. Chem. Eng., 2019, **7**, 13105-13114.

7 D. Chinnadurai, R. Rajendiran, O. Li and K. Prabakar, Appl. Catal., B, 2021, **292**, 120202.

8 Y. Lu, C. Yue, Y. Li, W. Bao, X. Guo, W. Yang, Z. Liu, P. Jiang, W. Yan, S. Liu, Y. Pan and Y. Liu, Appl. Catal., B, 2021, **296**, 120336.

9 J. Wang, M. Zhang, G. Yang, W. Song, W. Zhong, X. Wang and M. Wang, Adv. Funct. Mater., 2021, **31**, 2101532.

10 M. Ma, J. Xu, H. Wang, X. Zhang, S. Hu, W. Zhou and H. Liu, Appl. Catal., B, 2021, **297**, 120455.

11 J. Wang, W.i Fang, Y. Hu, Y. Zhang, J. Dang, Y. Wu, B. Chen, H. Zhao and Z. Li, Appl. Catal., B, 2021, **298**, 120490.

12 D. Cao, H. Xu and D. Cheng, Appl. Catal., B, 2021, **298**, 120600.

13 H. Liu, J. Cheng, W. He, Y. Li, J. Mao, X. Zheng, C. Chen, C. Cui and Q. Hao, Appl. Catal., B, 2022, **304**, 120935.

14 L. Tan, J. Yu, H. Wang, H. Gao, X. Liu, L. Wang, X. She and T. Zhan, Appl. Catal., B, 2022, **298**, 120915.

15 Y. Xu, M. Liu, S. Wang, K. Ren, M. Wang, Z. Wang, X. Li, L. Wang and H. Wang, Appl. Catal., B, 2021, **298**, 120493.

16 B. Liu, Y. Cheng, B. Cao, M. Hu, P. Jing, R. Gao, Y. Du, J. Zhang and J. Liu, Appl. Catal., B, 2021, **298**, 120630.

17 W. Li, J. Liu, P. Guo, H. Li, B. Fei, Y. Guo, H. Pan, D. Sun, F. Fang and R. Wu, Adv. Energy Mater., 2021, **11**, 2102134.

18 P. Wei, X. Li, Z. He, Z. Li, X. Zhang, X. Sun, Q. Li, H. Yang, J. Han and Y. Huang, Appl. Catal., B, 2021, **299**, 120657

19 Y. Feng, Z. Li, C. Cheng, W. Kang, J. Mao, G. Shen, J. Yang, C. Dong, H. Liu and X. Du, Appl. Catal., B, 2021, **299**, 120658.

20 Y. Gao, Z. Chen, Y. Zhao, W. Yu, X. Jiang, M. He, Z. Li, T. Ma, Z. Wu and L. Wang, Appl. Catal., B, 2022, **303**, 120879.

21 S. Yang, J. Zhu, X. Chen, M. Huang, S. Cai, J. Han and J. Li, Appl. Catal., B, 2022, **304**, 120914.

22 J. Chen, Q. Long, K. Xiao, T. Ouyang, N. Li, S. Ye and Z. Liu, Sci. Bull., 2021, **66**, 1063-1072.

23 Q. Zhang, W. Xiao, W. Guo, Y. Yang, J. Lei, H. Luo and N. Li, Adv. Funct. Mater., 2021, **31**, 2102117.

24 J. Zhang, Y. Yan, B. Mei, R. Qi, T. He, Z. Wang, W. Fang, S. Zaman, Y. Su, S. Ding and B. Xia, Energy Environ. Sci., 2021, **14**, 365-373.

25 K. Yue, J. Liu, Y. Zhu, C. Xia, P. Wang, J. Zhang, Y. Kong, X. Wang, Y. Yan and B. Xia, Energy Environ. Sci., 2021, **14**, 6546.

26 H. Xu, H. Shang, C. Wang, L. Jin, C. Chen, C. Wang and Y. Du, Appl. Catal., B, 2020, **265**, 118605.

27 Y. Lu, D. Fan, Z. Chen, W. Xiao, C. Cao and X. Yang, Sci. Bull., 2020, **65**, 460-466.

28 Z. Chen, Y. Ha, H. Jia, X. Yan, M. Chen, M. Liu and R. Wu, Adv. Energy Mater., 2019, **9**, 1803918.

29 H. Zhang, Y. Lv, C. Chen, C. Lv, X. Wu, J. Guo and D. Jia, Appl. Catal., B, 2021, **298**, 120611.

30 L. Sun, Z. Dai, L. Zhong, Y. Zhao, Y. Cheng, S. Chong, G. Chen, C. Yan, X. Zhang, H. Tan, L. Zhang, K. N. Dinh, S. Li, F. Ma and Q. Yan, Appl. Catal., B, 2021, **297**, 120477.

31 Z. Shi, J. Zhao, C. Li, H. Xu and G. Li, Appl. Catal., B, 2021, **298**, 120558

32 G. Yuan, J. Bai, L. Zhang, X. Chen and L. Ren, Appl. Catal., B, 2021, **284**, 119693.

33 Q. Qian, Y. Li, Y. Liu and G. Zhang, Appl. Catal., B, 2020, **266**, 118642.

34 X. Luo, P. Ji, P. Wang, R. Cheng, D. Chen, C. Lin, J. Zhang, J. He, Z. Shi, N. Li, S. Xiao and S. Mu, Adv. Energy Mater., 2020, **10**, 1903891.

35 T. Gong , J. Zhang, Y. Liu, L. Hou, J. Deng and C. Yuan, Chem. Eng. J., 2023, **451**, 139025.

36 S. Lim, C. Chiang, C. Peng, W. Wu, Y. Lin, Y. Lin, C. Chen and Y. Lin, Chem. Eng. J., 2023, **452**, 139715.

37 K. Ding, J. Hu, W. Jin, L. Zhao, Y. Liu, Z. Wu, B. Weng, H. Hou and X. Ji, Adv.

Funct. Mater., 2022, **32**, 2201944.

38 L. Jia, G. Du, D. Han, Y. Wang, W. Zhao, Q. Su, S. Ding and B. Xu, Chem. Eng. J., 2023, **454**, 140278.

39 L. Tan, J. Yu, H. Wang, H. Gao, X. Liu, L. Wang, X. She and T. Zhan, Appl. Catal., B, 2022, **303**, 120915.

40 P. Sun, Y. Zhou, H. Li, H. Zhang, L. Feng, Q. Cao, S. Liu, T. Wågberg and G. Hu, Appl. Catal., B, 2022, **310**, 121354.

41 G. Kresse, J. Furthmüller and Comput. Mater. Sci., 1996, **6**, 15-50.

42 G. Kresse and J. Furthmüller, Matter Mater. Phys., 1996, **54**, 11169-11186.

43 M. Gajdoš, K. Hummer, G. Kresse, J. Furthmüller and F. Bechstedt, Matter Mater. Phys., 2006, **73**, 045112.

44 A. D. Becke, J. Chem. Phys., 1993, **98**, 5648-5652.

45 J. P. Perdew, J. A. Chevary, S. H. Vosko, K. A. Jackson, M. R. Pederson, D. J. Singh and C. Fiolhais, Matter Mater. Phys., 1992, **46**, 6671-6687.

46 M. Ernzerhof and G. E. Scuseria, J. Chem. Phys., 1999, **110**, 5029-5036.

47 J. C. Sancho-García, J. L. Brédas and J. Cornil, Chem. Phys. Lett., 2003, **377**, 63-68.

48 W. Li, L. Kong, C. Chen, J. Gou, S. Sheng, W. Zhang, H. Li, L. Chen, P. Cheng and K. Wu, Sci. Bull., 2018, **63**, 282-286.

49 S. Grimme, J. Antony, S. Ehrlich and H. Krieg, J. Chem. Phys., 2010, **132**, 154104.

50 S. Grimme, S. Ehrlich and L. Goerigk, J. Comp. Chem., 2011, **32**, 1456-1465.